

Parameters of thermal performance of plaster blocks: Experimental analysis

 P.I.B. Batista ^a,  J.H.A. Rocha ^b✉,  Y.V. Póvoas ^a

a. University of Pernambuco, (Recife, Brazil)
b. Federal University of Rio de Janeiro, (Rio de Janeiro, Brazil)
✉: joaquin.rocha@coc.ufrj.br

Received 4 August 2022
Accepted 31 December 2022
Available on line 24 May 2023

ABSTRACT: This work aims to obtain parameters of thermal performance of various types of plaster blocks for vertical sealing. The methodology consisted of making test elements with 8 types of plaster blocks, in addition to plasterboard of different densities. Thermal resistance, transmittance, capacity, and delay were calculated, according to the Brazilian standard NBR 15220. Thermal behavior tests were carried out with controlled heating through a heat source, digital thermometer, infrared thermography, and an instrumented thermal chamber developed for this work. The experimental results corroborated with the trend indicated by the calculated parameters. The massive and hollow blocks of 100 mm had the best results followed by the 76 mm hollow blocks. The 50- and 70-mm massive blocks were among those with the worst thermal behavior. The study through the thermal chamber and real test elements associated with the normative methods allowed the practical verification regarding the thermal behavior of the components.

KEY WORDS: Plaster block; Thermal chamber; NBR 15220; Infrared thermography.

Citation/Citar como: Batista, P.I.B.; Rocha, J.H.A.; Póvoas, Y.V. (2023) Parameters of thermal performance of plaster blocks: Experimental analysis. *Mater. Construcc.* 73 [350], e314. <https://doi.org/10.3989/mc.2023.299322>.

RESUMEN: *Parámetros del comportamiento térmico de bloques de yeso: análisis experimental.* Este trabajo tiene como objetivo obtener parámetros de desempeño térmico de varios tipos de bloques de yeso para sellado vertical. La metodología consistió en realizar elementos de prueba con 8 tipos de bloques de yeso, además de placas de yeso laminado de diferentes densidades. Se calcularon la resistencia térmica, la transmitancia, la capacidad y el retardo, de acuerdo con la norma brasileña NBR 15220. Se realizaron pruebas de comportamiento térmico con calentamiento controlado a través de una fuente de calor, termómetro digital, termografía infrarroja y una cámara térmica instrumentada desarrollada para este trabajo. Los resultados experimentales corroboraron la tendencia indicada por los parámetros calculados. Los bloques macizos y huecos de 100 mm presentaron los mejores resultados seguidos de los bloques huecos de 76 mm. Los bloques macizos de 50 y 70 mm estaban entre los de peor comportamiento térmico. El estudio con cámara térmica y elementos de prueba reales asociados a los métodos normativos permitió la verificación práctica en cuanto al comportamiento térmico de los componentes.

PALABRAS CLAVE: Bloque de yeso; Cámara térmica; NBR 15220; Termografía infrarroja.

Copyright: ©2023 CSIC. This is an open-access article distributed under the terms of the Creative Commons Attribution 4.0 International (CC BY 4.0) License.

1. INTRODUCTION

In recent years, Brazil has followed the global trend of modernization and improvement in the construction industry, including in terms of thermal performance. Through a new standardization to verify the performance of residential buildings, the Brazilian construction industry enters a new regulatory level that will require new technologies to optimize the results of its products and services. In the European Union, the regulations aim at the construction of energy efficient buildings to improve people's quality of life and generate additional benefits to the economy and society (1).

The interaction of the building with the environment in which it is located is important to fully meet the needs of users through the optimization of its functionalities. Accurate knowledge of the properties and thermal behavior in building elements under typical conditions is essential for innovative products and techniques. It may optimize current projects and produce more accurate data for the cost-benefit analysis for future projects (2-5).

Ascione *et al.* (6) highlight that the use and development of construction components characterized by values of thermal transmittance, thermal capacity, and radiative properties is a key strategy for reducing the need for energy for microclimate control. The thermal behavior of a building has intervening factors: the climate, thermal physiology of the users, and even the processes of heat transmission, which are directly linked to the building elements, especially floors, roofs, and facades (7-9).

According to Pereira (10), the quality of a building is no longer assessed by looking only at architectural, structural, or installation projects. The comfort component of users is increasingly demanded both by the users themselves and by councils and supervisory bodies, especially through rules and regulations (11). According to Aguilera *et al.* (12), the current century will be one of energy efficiency in buildings, as shown by the appearance of many national and international guidelines in recent years, such as the European 20/20/20 objectives, in which a 20% reduction in the energy consumption in buildings is established for the year 2020. In this sense, the European Commission in 2021, to promote the energy efficiency of buildings, established a review of the Energy Performance of Buildings Directive (EPBD), proposing a regulatory framework. This improvement includes five general EPB standards: a) ISO 52000-1 (13), is the general framework of EPB evaluation; b) ISO 52003-1 (14), information for processing the results of the EPB standards, resulting into general and partial indicators; c) ISO 52010-1 (15), procedures for evaluation of climatic data; d) ISO 52016-1 (16), guidelines for calculating temperatures and energy needs, and e) ISO 52018-1 (17), description of the indicators for specific EPB requirements.

Tubelo *et al.* (18) as well as Bogo (19) affirm that the advances in norms, regulations, and patterns of energy use have an important role to play in supporting the construction of superior quality houses, which are more thermally comfortable and economical power. The Brazilian mandatory legal standards NBR 15220 (20) and NBR 15575 (21), and, in an informative way, the Technical Quality Regulation for the Energy Efficiency Level Residential Buildings (RTQ-R) (22), are the support legal instruments in Brazil.

Two normative procedures are established by NBR 15575 (21): the simplified and computer simulation method. The first consists of calculating and observing parameters of the thermal behavior of the systems and comparing them with the minimum allowable values. The second procedure should be used if the building does not meet the requirements of the simplified method (minimum performance) or if it is desired to achieve intermediate and higher performance (21, 23, 24). In addition to these procedures, there is the experimental measurement method where measurements are made on buildings or prototypes built.

Experimental studies of construction elements, especially vertical sealing blocks, have been carried out to evaluate their thermal properties (25-33). The use of thermal chambers that simulate the environments in a thermal gradient assesses the behavior of the components experimentally. It is a practical method that has shown significant results, especially for the comparison of components of different materials, such as ceramic and concrete blocks with substitution of fine aggregates by residues of Ethyl Vinyl Acetate from the shoe industry (30). For clay bricks, Allam *et al.* (31) developed a thermal chamber and performed heat and humidity flow tests based on the control and reproduction of various environmental conditions. Specht *et al.* (28) built a chamber to test prototypes of walls and perform, in parallel, mathematical simulations to evaluate the experimental results on the heat flow to walls of different materials.

Infrared thermography is not yet an established method for assessing the performance and thermal behavior of buildings and is not present in the relevant Brazilian standards NBR 15220 (20) and NBR 15575 (21). However, some studies verify the potential of the use of thermography (6, 10, 12, 23, 32-39), both (a) for measuring parameters of thermal properties for the elements and the building, and (b) to find problems related to thermal bridges and the overall performance of the building.

A thermal performance study is critical for construction sector, especially in developing countries where more energy may be consumed than in developed countries (40). However, a unique method to evaluate thermal performance in plaster composite materials is unavailable. In this context, ways to measure and estimate thermal properties in plaster

composite materials have been proposed by literature (41-44). Those studies have suggested using thermal chambers (45, 46), specific equipment (47-49) and infrared thermography (50). As mentioned by Batista (51), there is a small amount of research that considers the plaster block for a vertical sealing element and a smaller amount evaluating it in thermal behavior, associated with the equally minimal mention of these elements in the relevant Brazilian standards reflect the importance of greater research in this sense (52-56).

This article aims to evaluate the main thermal properties of plaster blocks from theoretical calculations and using thermal chamber and infrared thermography as experimental methods, considering the technical and economic potential of these elements for the economy of the northeast region of Brazil. The experimental program included the development of a thermal chamber with sensors, a digital thermometer, a heat source with intensity control, in addition to having a compatible format for infrared thermography, the latter for capturing thermal images during tests. This combination allowed for a broad, original, and data-rich analysis for thermal performance in testing elements.

2. MATERIALS AND METHODS

To evaluate the thermal properties of plaster blocks, three analysis fronts were performed: one theoretical, based on the simplified method; one determined by test – both proposed by NBR 15220 (20); and an ex-

perimental study from an instrumented thermal chamber developed for this work. Methodology used for this research is detailed in Figure 1.

2.1. Test elements

From plaster blocks standardized by NBR 16494 (57), eight test elements were produced, covering the different thicknesses for the configurations available between hollow and compact in the Brazilian market. The main characteristics are presented in Table 1.

Both chemical and physical characteristics used in manufacturing plaster blocks are shown in Table 2.

Every plaster block was manufactured in an industrial manner, including cubical metal molds (solid and hollow) with smooth surface and side fits. Subsequently, plaster blocks were dismounted after 60 min and taken to an oven at 40 °C for 24 hours, according to NBR 16494 (57). It is worth mentioning that test elements are from the plaster block cuts provided by the industry. Therefore, their lateral dimensions were changed to a 42 cm square on the side, inserting the identification acronym and the Type K thermocouple temperature sensors in the central part on both sides of the test elements (Figure 2).

Figure 3 presents the mechanical properties of the plaster specimens. The flexural strength of the blocks meets the requirements of NBR 16494 (57). The compressive strength was determined by ABNT 12129 (60), using cubic specimens of 50 cm x 50 cm x 50 cm.

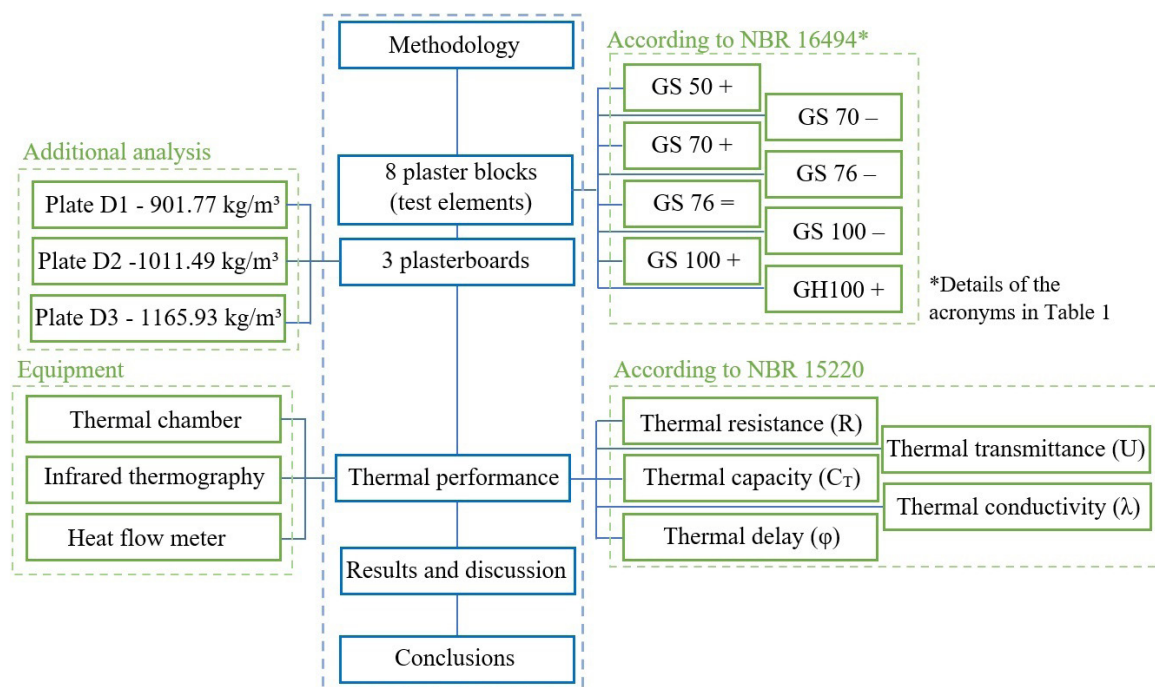
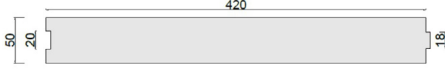
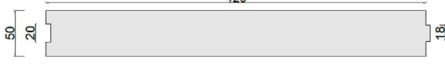
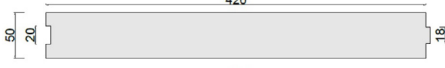
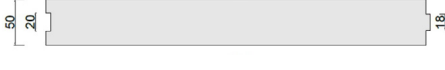



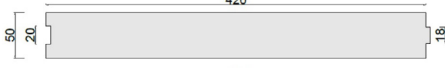


FIGURE 1. Methodology.

TABLE 1. Test elements in plaster blocks.

Code	Type	Internal structure (all dimensions in mm)	Water/plaster ratio (w/p)	Flexural strength MPa	Apparent mass density range
GS 50 +	Standard	Compact	0.72	1	Average ¹
					
GS 70 -	Standard	Hollow - conical	0.70	1.2	Average ¹
					
GS 70 +	Standard	Compact	0.70	1.2	Average ¹
					
GS 76 -	Standard	Hollow - conical	0.68	1.4	Average ¹
					
GS 76 =	Standard	Hollow - cylindrical	0.68	1.4	Average ¹
					
GS 100 -	Standard	Hollow - conical	0.65	1.5	Average ¹
					
GS 100 +	Standard	Compact	0.65	1.5	Average ¹
					
GH 100 +	Hydrofugated ²	Compact	0.65	1.5	Average ¹
					

¹Average density: ≥ 800.0 and < 1100.0 kg / m³, according to NBR 16494 (57).

² Hydrofugate: Hydrofugate blocks with water absorption $\leq 5.0\%$, according to NBR 16494 (57).

TABLE 2. Chemical and physical characteristics of plaster.

Characteristics	Plaster	Requirement	Brazilian Standards
Calcium oxide - CaO (%)	39.8	>38.0	NBR 13207 (58)
Sulfuric anhydride - SO ₃ (%)	55.1	>55.0	NBR 13207 (58)
Crystallization water (%)	5.97	4.2 - 6.2	NBR 13207 (58)
Fineness modulus	0.18	<1.1	NBR 12127 (59)
Unit mass (kg/m ³)	610	<700	NBR 12127 (59)

Data provided by manufacturer.



FIGURE 2. Details of the test elements in front and perspective view.

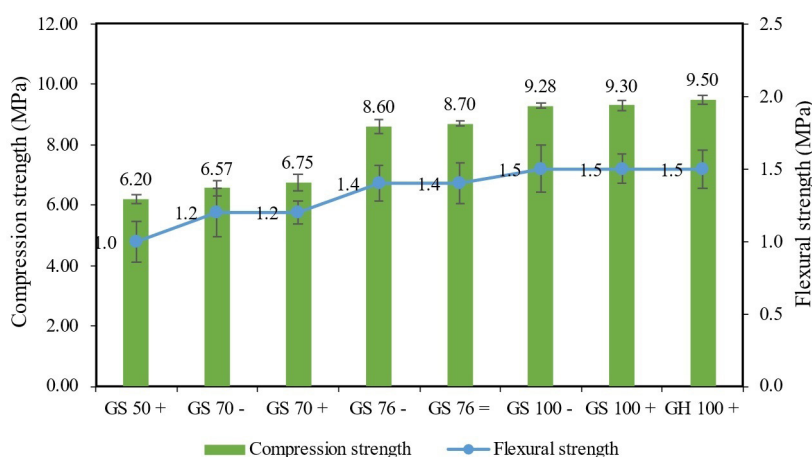


FIGURE 3. Mechanical performance of the plaster specimens.

2.2. Thermal chamber

In order to carry out the thermal chamber behavior experiment, a thermal chamber was developed and built to provide the test element with the positioning between two environments with a temperature gradient between them (25, 28, 31). The test apparatus was built of wood, with insulation on the heated side and opening on the cold side (controlled room temperature). In addition, temperature sensors were inserted on both sides with a display on the control panel. A dimmer switch was also inserted to regulate the heating provided by an infrared lamp present in the central part of the hot side and the location for installing the digital thermometer with integrated data logger (Figure 4). Although there is no official standard, a proposed thermal chamber was developed according to Standard ASTM C1363 (61) provisions and studies by Kheradmand et al. (45), Pedreño-Rojas et al. (46), and Ferrari and Zanotto (62). The thermal chamber was used for temperature monitoring through thermal sensors. Additionally, elements' surface temperature distribution was evaluated through infrared thermography.

The procedure of the experiment consists of controlling the temperature in the environment: 26 ± 1 °C, from an air conditioner. Then, the test elements are placed with the “outer face” turned to the inside the chamber. Strips of expanded polystyrene are placed on the edges the sensors are connected, the data logger is programmed, and heating is started. The heating lasts 360 minutes. Thermograms are recorded every 60 minutes on the cold side of the test elements and the temperatures are recorded every minute. After the warm-up period, the test elements cool for 120 minutes, with the same rate of temperature recording by the sensors. However, thermograms are made every 30 minutes and in various positions (cold side, hot side, lateral, and perspective) to observe the heat transition in the test element. The follow-up used the FLIR E-60 equipment, with main characteristics are shown in Table 3.

The emissivity values of the analyzed surfaces were found using the black layer method. Interaction was performed between the emissivity value of the tape - known - and that of the neighboring surface (material, whose emissivity is unknown) un-



FIGURE 4. Details of the apparatus developed for the thermal chamber behavior experiment.

TABLE 3. Characteristics of the FLIR E-60 thermal camera.

Model FLIR E-60	
IR resolution	320x240 pixels
Thermal Sensitivity	< 0.05°C
Temperature range	-20 and 650 °C
Accuracy	± 2°C or ± 2%
Video camera (no backlit)	3.1 MP

Source: FLIR (63).

til the temperatures coincide. Values between 0.93 and 0.95 were found for the plaster. The distance to the object was always between 1.0 and 1.5 m. The reflected temperature was the same as that of the environment, with no interference in the results (no interference from sunlight, variation in lighting, or considerable temperature in the controlled environment).

2.3. Heat flow meter

The NBR 15220 standard (20) recommends the performance of tests to determine the thermal resistance of elements. One of the methods mentioned is the flow meter; the test is based on ISO 8301. For this research, the Netzsch heat flow meter - HFM

TABLE 4. Characteristics of the heat flow meter.

Model NETZSCH - HFM 436/6	
Temperature range	-20 ~ 70 °C
Cooling system	External cooler
Specimen size	600 x 600 x 10 ~ 200 mm
Detectable area of the heat flow transducer	25.4 cm x 25.4 cm
Range for thermal resistance	0.1 ~ 8.0 m ² K/W
Thermal conductivity range	0.005 ~ 0.50 W/m·K
Accuracy	±1 ~ 3%
Repeatability	0.50%

Source: NETZSCH (65).

436/6 was used, with main characteristics presented in Table 4. Tests were performed under the steady-state heat transfer, using the absolute technique, detailed by Zhao *et al.* (64).

To carry out this test, the wells of the hollow blocks were closed with plaster paste, with the aid of a glass plate to prevent heat loss from the sides. It is noteworthy that the size of the test elements (42 cm x 42 cm) is compatible and still have a margin in relation to the detectable area of the heat flow transducer (25.4 cm x 25.4 cm) (Table 4). In addition to the tests on plaster blocks - all belonging to the medium density range as shown in Table 1 -, 3 plaster plates had the exact size of the equipment's specimen (60 cm x 60 cm x 5 cm). The plates are D1 - 901.77 kg/m³, D2 - 1011.49 kg/m³ and D3 - 1165.93 kg/m³: two distant points but within the average range (between 800 and 1100 kg/m³) and one point within the high-density range (greater than 1100 kg/m³), according to NBR 16494 (57). The plasterboards were tested to have a greater range of results, considering that the plates were made specifically for the size of the equipment (60 cm x 60 cm). In addition, the plasterboards are made of a homogeneous material, which makes it possible to better infer thermal conductivity, based on the relationship between thermal resistance and the thickness of the test specimen.

The test was carried out according to the recommendations of the NBR 15520 standard (20) and the manufacturer's recommendations (65). For the test with the 8 plaster block test elements, two main temperature values were used - Mean T of 24 and 40 °C - referring to a temperature close to the environment in part of Brazil and a higher one representing a peak during summer or artificial warming situations. On the other hand, for the plasterboard, in addition to these main temperatures, other two higher ones (50 and 60 °C) were added to expand the analysis of plaster, considering thermal conductivity (λ) under density conditions of apparent mass present in this work.

2.4. Characteristics of the heat flow meter

To obtain theoretical thermal properties for test elements, calculations of several parameters were performed according to prescriptions and tabulated input data values present in NBR 15220 (20). Among the input data values collected, the following stand out for the plaster: specific heat (c) of 0.84 kJ/kg·K, thermal conductivity (λ) of 0.35 W/m·K, and apparent mass density (ρ) of 875.0 kg/m³. The calculations were performed with the aid of spreadsheets programmed in the PTC Mathcad and MS Excel software. The calculated parameters were thermal resistance (R) (Equation [1] and Equation [2]), thermal transmittance (U) (Equation [3]), thermal capacity (C_T) (Equation [4]), and thermal delay (ϕ)

(Equation [5]).

$$R = e/\lambda \quad [1]$$

$$R_T = R_{SI} + \sum_j R_j + R_{SE} \quad [2]$$

$$U = 1/R_T \quad [3]$$

Here, e is the layer thickness (m); λ is the thermal conductivity (W/m·K); R_T is the total thermal resistance (m²·K/W); R_j is the thermal resistance of each component layer (m²·K/W); R_{SI} is the internal surface thermal resistance (m²·K/W), and R_{SE} is the external surface thermal resistance (m²·K/W).

$$C_T = \sum_j \lambda_j \cdot R_j \cdot c_j \cdot \rho_j = \sum_j e_j \cdot c_j \cdot \rho_j \quad [4]$$

Here, λ_j is the thermal conductivity of each component layer (W/m·K); R_j is the thermal resistance of each component layer (m²·K/W); c_j is the material specific heat of each component layer (kJ/kg·K); ρ_j is the apparent mass density of each component layer (kg/m³), and e_j is the layer thickness of each component layer (m).

$$\varphi = 1.382 \cdot R_t \cdot \sqrt{0.226 \cdot \frac{C_T - C_{EXT}}{R_t} + 0.205 \cdot \frac{(\lambda \rho c)_{EXT}}{R_t} \cdot (R_{EXT} - \frac{R_t - R_{EXT}}{10})} \quad [5]$$

Here, R_t is the surface to surface thermal resistance (m²·K/W); λ is the thermal conductivity of the material (W/m·K); c is the material specific heat (kJ/kg·K); ρ is the apparent mass density of the material (kg/m³), and R_{EXT} is the thermal resistance of the component's outer layer (m²·K/W).

3. RESULTS AND DISCUSSION

The discussion of the results is presented for each of the three analyzes carried out.

3.1. Thermal Resistance (R) and Thermal Conductivity (λ)

Flow meter measured the thermal resistance and based on the thickness of the specimen, calculates the thermal conductivity (in case of homogeneous material). The values found for thermal conductivity corroborate with the value suggested in NBR 15220 (20), which is 0.35 W/m·K for a temperature of 27 °C (20). For densities D1, D2, and D3, the values for temperature 24 °C were 0.358 W/m·K, 0.354 W/m·K, and 0.364 W/m·K, respectively. The value suggested in the standard, therefore, can be used if testing is not available, according to the presented results. The values of R and λ for each of the main temperatures are in Table 5.

It should be noted that the variation in the conductivity value with temperature occurs in a more

sensitive way when this difference is high in most materials (66).

For the nominal main temperature of 24 °C (SP#1 in Table 5), there is slight variation in conductivity in relation to the density of the material. However, for higher temperatures, an increase in thermal conductivity occurred with a decrease in the density of apparent mass. This situation differs from the results pointed out by Souza (27) who concluded in his study that the increase in the porosity of plaster specimens with the addition of sodium bicarbonate caused the decrease in thermal conductivity. The author also states that heat transfer through pores are slow processes and that the stagnant air, usually present inside the pores, is a bad heat conductor ($\lambda = 0.02$ W/m·K); when isolated, they make gas convection difficult (27).

TABLE 5. Plasterboard Thermal conductivity – Flow meter.

Test element	Measured thickness ¹ cm	Calculated density kg/m ³	SP ² #	Main temperature °C	Thermal conductivity (λ) W/m·K
Plate D1	5.20	901.77	1	25.31	0.358
			2	39.84	0.403
			3	49.64	0.409
			4	59.43	0.405
Plate D2	5.21	1011.49	1	22.33	0.354
			2	40.17	0.368
			3	49.92	0.372
			4	59.75	0.365
Plate D3	5.21	1165.92	1	22.38	0.364
			2	40.17	0.368
			3	49.85	0.361
			4	59.60	0.356

¹Thickness provided by the flow meter during the test.

²Set point - Test data collection point.

The temperature affects the thermal conductivity of ceramic materials, the increase in temperature (in this case up to 60 °C) can explain the increase in thermal conductivity. On the other hand, porosity also has a direct influence, the increase in volume and/or number of pores reduces the thermal conductivity of ceramic materials (67, 68). In this case, based on the results presented, the higher temperatures of the test had more influence than the porosity on the thermal conductivity; however, a detailed study about the phenomena involved could better define this behavior.

Regarding the test elements from plaster blocks, Table 6 shows results and details for the apparent mass density, with specific value for each tested element. Results confirmed the trend of less thick

blocks (GS 50 +, GS 70 + and GS 70 -) to have the lowest R values. Among the blocks of 100 mm thick, those massive (GH 100 + and GS 100 +) presented lower values than the hollow ones (GS 100-) and even lower values than both 76 mm hollow blocks (GS 76 - and GS 76 =). It highlights the significant contribution of the air layer (alveoli) inside these blocks to the increase of thermal resistance, even with the reduction of the total thickness. Similar results were reported when thermal resistance for hollowed-block walls was evaluated (44, 69). The values of the standard 100 mm compact, water repellent compact, and standard hollow blocks ranged between 0.25 and 0.30 m²·K/W, while both 76 mm blocks performed with R around 0.29 m²·K/W.

The values of heat flow for the plaster block test elements are also graphically presented in ascending order for the two main temperatures of 24 °C and 40 °C (Figure 5). Thermal resistance is not significantly modified by temperature (up to 40 °C). However, Mansour *et al.* (70) points out that higher temperatures (above 100 °C) may cause the plaster work as a firebreak.

3.2. Thermal performance parameters

Table 7 presents the results of the thermal performance parameters calculated as indicated in NBR 15220 (20) for the 8 plaster block test elements.

Analyzing the thermal resistance value, calculated from the presence of the alveoli in the plaster blocks, it is observed that this causes an increase in the thermal resistance value when compared to the compact ones (solid). An increase of 14% is observed between the 70 mm blocks while it's only 3% for the 100 mm blocks. This difference in magnitude in the increase between the 70 and 100 blocks is due to the greater influence of the alveoli size in relation to their total thickness in the less thick block – since the alveoli have the same size. However, this

TABLE 6. Thermal resistance values for plaster blocks – flow meter.

Test element	Measured thickness ¹ cm	Calculated density kg/m ³	SP ² #	Main temperature °C	Thermal resistance (R) m ² ·K/W
GS 50 +	5.1999	871.2	1	25.06	0.163
			2	39.66	0.168
GS 70 +	7.0259	999.3	1	24.87	0.192
			2	39.19	0.202
GS 100 +	10.0802	978.6	1	24.76	0.260
			2	38.54	0.270
GH 100 +	9.9942	991.0	1	24.78	0.248
			2	38.82	0.262
GS 70 -	6.9812	812.8	1	23.98	0.219
			2	40.23	0.229
GS 76 -	7.5551	822.8	1	25.04	0.295
			2	39.22	0.298
GS 76 =	7.5567	867.2	1	25.28	0.287
			2	39.89	0.283
GS 100 -	10.1819	960.4	1	25.34	0.300
			2	39.31	0.298

¹Thickness provided by the flow meter during the test.

²Set point - Test data collection point.

behavior does not happen between elements with 76 mm plaster blocks, where there is a decrease in the resistance for the block with the largest alveolus (GS 76 =) – around 3% (Figure 6).

The “removal” of solid material from the blocks proved to be an alternative to increase the total re-

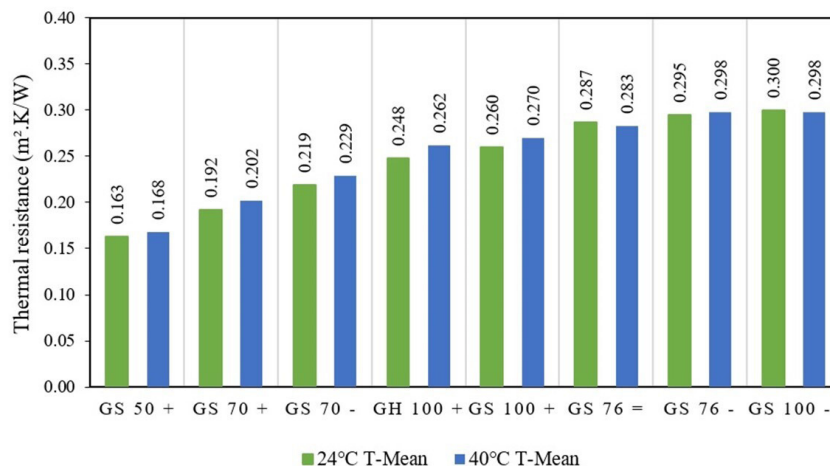


FIGURE 5. Graph of thermal resistance measured using a flow meter.

TABLE 7. Thermal performance parameters for plaster blocks - NBR 15220 (20).

Test element m ² ·K/W	Thermal resistance (R) m ² ·K/W	Total thermal resistance (R _T) ¹ W/m ² K	Thermal transmittance (U) kJ/m ² ·K	Thermal capacity (C _T) h	Thermal delay (φ)
GS 50 +	0.143	0.313	3.19	37	1.7
GS 70 +	0.200	0.370	2.70	59	2.5
GS 100 +	0.286	0.456	2.19	82	3.5
GH 100 +	0.286	0.456	2.19	83	3.5
GS 70 –	0.228	0.398	2.51	41	1.9
GS 76 –	0.248	0.418	2.39	37	1.8
GS 76 =	0.240	0.410	2.44	28	1.5
GS 100 –	0.294	0.464	2.15	51	2.3

¹Considering the surface resistance plots (RSI + RSE = 0.170): value used to calculate U.

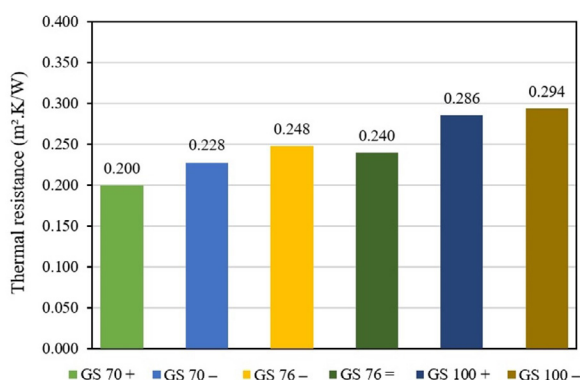


FIGURE 6. Graph of thermal resistance (R) based on the alveoli.

sistance, as seen in the results of the flow meter (Table 6 and Figure 5). Evidence shows less thick hollow blocks with results superior to other thicker blocks. As mentioned by Zhang et al. (71), hollow blocks improve thermal insulation properties in walls (mainly thermal resistance) and reduce energy consumption. This is caused by thermal resistance of air contained in the block. However, the amount of reduction in plaster thickness presented in the “popular block”, material for the “GS 76 =” element, resulted in a decrease in thermal resistance since the calculation considers a fixed value for the resistance of the air layer: if it is increased, the only practical effect is to reduce the thickness of the solid material and, consequently, decrease its contribution to the element thermal resistance.

Thermal transmittance (U) and thermal capacity (C_T) are two criteria analyzed by the building performance standard NBR 15575 (21) for external vertical sealing systems. This work points out that usually compartmentalization of environments, as to thermal aspects, is needed. Therefore, it is important to understand the properties of the blocks as one of the components in sealing systems, both external and

internal (the latter more common for plaster blocks).

Figure 7 presents a joint graph of these parameters.

For the bioclimatic zone 8 (20) minimum values of C_T are not required, while in the other zones (1 to 7) at least 130 kJ/m²·K is imperative for minimum thermal performance, according to NBR 15575 (21). In addition, for U appreciation it is necessary to know the absorption to solar radiation (α), which is related to the last outer layer of the External Vertical Sealing System. Therefore, for the plaster block test elements (without coating), this analysis, according to the normative requirements, is not relevant. However, it is interesting to note that the test elements in solid plaster blocks (GS 100 + and GH 100 +) presented the best combination of results: low U values - around 2.2 W/m²·K - and C_T - about 82 kJ/m²·K. All test elements with thicknesses from 76 mm show U values within the requirements of any of the bioclimatic zones for walls (U ≤ 2.5), even without coatings, which significantly improve these values (blue line in Figure 7). The minimum C_T value (130 kJ/m²·K) for zones 1 to 7 corresponds to the orange line (Figure 7).

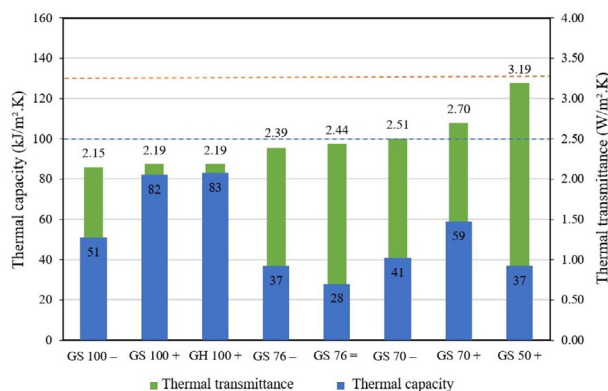


FIGURE 7. Graph of thermal transmittance (U) and thermal capacity (C_T).

Although the thermal transmittance (U) values are higher than those reported by Bianco *et al.* (72) (0.56-0.8 $W/m^2 \cdot K$) and Asdrubali *et al.* (73) (0.23-0.33 $W/m^2 \cdot K$) testing conditions and material settings were different. In previous studies, tests were carried out in situ and coating was included.

For thermal delay (ϕ), test elements with greater thickness and less voids present, in general, the highest values, as reported by Simões *et al* (74) and Tadeu *et al.* (75). This statement is even clearer when observing the test elements of the same thickness, with a difference only in the presence and size of the alveoli. Among the test elements with 100 mm, there is a 44% reduction between the massive one (3.5 h) and the hollow sample (2.3 h); for the 70 mm (GS 70 - and GS 70 +) blocks, there is 1.9 h for the hollow and 2.5 h for the similar compact. Finally, for

the 76 mm elements, the difference was only 0.3 h: 1.5 hrs for GS 76 = and 1.8 hrs for GS 76 -; the 50 mm block had a thermal delay slightly higher than the GS 76 =, with 1.7 h.

3.3. Thermal chamber

The average temperature evolution of both the cold and warm environments in the thermal chamber is shown in Figure 8. Values were collected every 60 minutes through the display located on the controller board (Figure 4); the room temperature sensors were positioned close to the surface of the test elements on both sides.

Figure 8 shows that increasing temperature also causes an increase in standard deviation, resulting

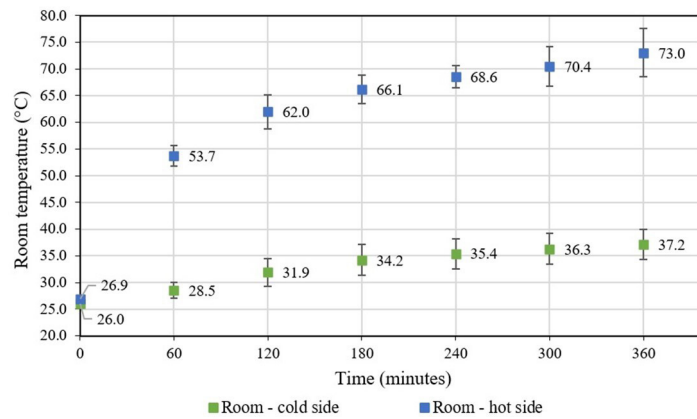


FIGURE 8. Graph of the average room temperature in the thermal chamber.

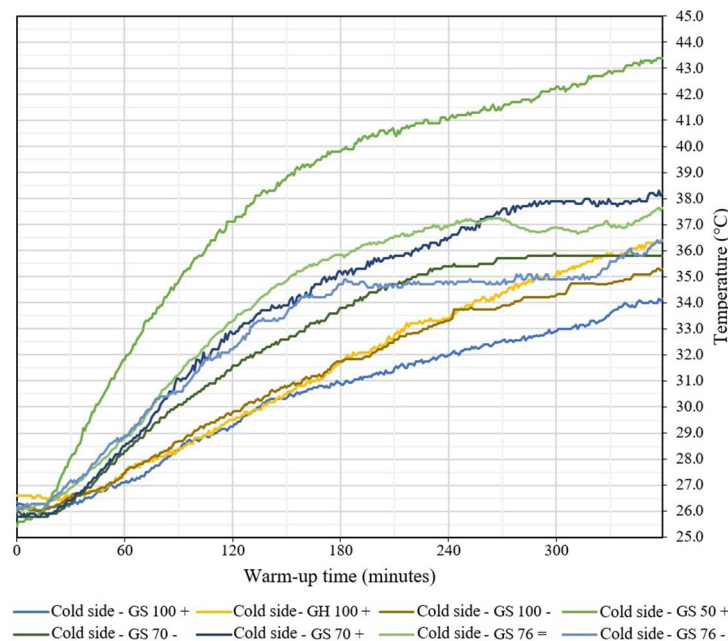


FIGURE 9. Experiment of thermal behavior in test elements – plaster blocks.

in greater variation, especially on the hot side of the chamber. Additionally, it was possible to compare the thermal behavior of the test elements in plaster block, since the variation occurred within an acceptable range, with a maximum value of 2.6 °C in the final minutes of heating. The graph for a 360-minute heating period for the 8 test elements is shown in Figure 9. In this graph, the control of the initial temperature is observed with values for all curves always within the range 26 ± 1 °C. The parameter most related to the thermal chamber behavior test is the thermal transmittance (U). To relate this parameter to the assay curves, Figure 10 presents a diagram where the test elements are on the sides in decreasing order for U value. In the central part, they are presented in the order of the curves for every 60 minutes.

However, one of the test elements, the GS 70 - (purple), shows less congruence in relation to the theoretical U value and its behavior during the test. Near 240 minutes, it presents a curve with very reduced acceleration and, therefore, almost no growth during the next 120 minutes (Figure 10). GS 76 - showed similar behavior. That happened especially between 180 and 300 minutes, with a possible state of balance between the room temperature on the cold side and the heat flow coming from the hot side. This situation may have been, in both cases, due to a cooling of the environment by the prolonged absence of operators, external climate, or even by distortions of the air conditioner thermostat. These situations were also indicated by Ferrari and Zanotto (62). Considering a trend in the curves of these two elements before the different points, in the final 60 minutes the relationship between U and the temperature on the cold side would probably be even clearer.

Relevant behavior is shown by the set of 100 mm blocks. The curves of the test elements GS 100 -, GH 100 + and GS 100 + remain isolated from the others between 40 and 260 minutes, returning to find the other hollow blocks (GS 70 -, GS 76) and approach the GS 76 = around 300 minutes. Behavior in 76 mm test elements should also be highlighted. It is important to note here that the difference between them is

only due to the thickness of the alveoli, which is about 25% greater in GS 76 =. Figure 10 shows the first 80 minutes of heating, both show a similar behavior; however, after that time, the curve of the block with the largest number of voids and the highest U value maintains the same acceleration, while the GS 76 - presents a deceleration over a period of 200 minutes. It will increase again only in the final stage, after 320 minutes. Both in the measured values of thermal resistance by the flowmetry method, as well as by the theoretical calculation, the thermal parameters of the GS 76 - proved to be superior to those of the GS 76 = and. In the test, such values were corroborated, despite the greater temperature difference between them: 2.5 °C for about 260 minutes of heating and at the end of the process, over 1 °C.

The GS 50 + showed little capacity to retain the heat passage during the test, in accordance with the theoretical values of its low thermal resistance, $R = 0.143$ and $R = 0.163$, calculated and measured, respectively. At the end of the process, there was almost 10 °C of temperature difference for the GS 100 +, which showed the best behavior, and 6 °C of difference for the second with the worst performance, the GS 70 +. The use of this block is restricted to decorations, cabinets, and small closings. It is rarely used for closing masonry. One possibility of use would be associated with a back layer to the ventilation layer in double walls, as it presents the characteristics common to plaster, such as flatness suitable for finishing, low density of apparent mass; it presents greater thickness and self-supporting capacity than plasterboard: dry-wall boards common thickness is 12.5 mm, and they need metal profiles for support.

Results obtained from the thermal chamber enable understanding thermal dynamic behavior and verifying theoretical values for tested plaster blocks. Previous studies have also established these thermal chamber advantages for plaster compounds (45, 46).

To complement the data collected by a digital thermometer, the thermograms made it possible to observe the distribution of heat by the test element during the heating period (Figures 11 and 12). By

Test element	U	Warm-up time (minutes)						Test element	U
		60	120	180	240	300	360		
GS 50 +	3.19	GS 50 +	GS 50 +	GS 50 +	GS 50 +	GS 50 +	GS 50 +	GS 50 +	3.19
GS 70 +	2.70	GS 76 -	GS 76 =	GS 76 =	GS 76 =	GS 70 +	GS 70 +	GS 70 +	2.70
GS 70 -	2.51	GS 76 =	GS 70 +	GS 70 +	GS 70 +	GS 76 =	GS 76 =	GS 70 -	2.51
GS 76 =	2.44	GS 70 +	GS 76 -	GS 76 -	GS 70 -	GS 70 -	GS 76 -	GS 76 =	2.44
GS 76 -	2.39	GS 70 -	GS 70 -	GS 70 -	GS 76 -	GH 100 +	GH 100 +	GS 76 -	2.39
GH 100 +	2.19	GH 100 +	GS 100 -	GS 100 -	GH 100 +	GS 76 -	GS 70 -	GH 100 +	2.19
GS 100 +	2.19	GS 100 -	GH 100 +	GH 100 +	GS 100 -	GS 100 -	GS 100 -	GS 100 +	2.19
GS 100 -	2.15	GS 100 +	GS 100 +	GS 100 +	GS 100 +	GS 100 +	GS 100 +	GS 100 -	2.15

FIGURE 10. Scheme of the relationship between the thermal behavior test and the U value.

the test element arrangement in the thermal chamber (bottom on the base of the chamber and the upper part with a gap for the top), there is a greater pre-disposition of heating in the upper part, aggravated by the lightness of the hot air that rises (76). The heat transfer to the base of the chamber by conduction promotes this lower temperature at the base of the test element, as seen in Figures 11 and 12. Although the expanded polystyrene strips have shown effectiveness in reducing the exchange of air between the hot and cold parts through the side and top cracks during the test, a possible improvement for the insulation is to make it closer to all the edges of the test elements, including the base.

The thermograms in Figures 11 and 12 corroborate the need to only use contact thermocouples in the central part of the test element, when heated by a point source, as mentioned in similar works (28, 30).

Figures 11 and 12 also indicate that the presence of the vertical alveoli (Figure 11) causes a more

vertical distribution of heat due to the transfer by convection that occurs within the air layer. On the other hand, in the solid element (Figure 12), a more radial distribution of the heat focus is clearly seen in the center due to the position of the heating lamp. Unlike the hollow element, where heat tends to rise between the alveoli, conduction allows the heating to be better distributed in the captured area, including the base (see part “6h” Figure 12). This situation can even explain the cause of the behavior of the GS 70 -; in the simulation it differs from the expected, when observing the values of its thermal parameters (Tables 6 and 7). Since the alveoli are open at the top through the gap between the test element and the roof of the thermal chamber, the exchange of hot air, even though it is hampered by the lateral closing and the use of polystyrene strips, occurred, and may have “part the heat flow” perpendicular to the face of the element for that point. Since the GS 70 - is the least thick hollow element, this circumstance affected its

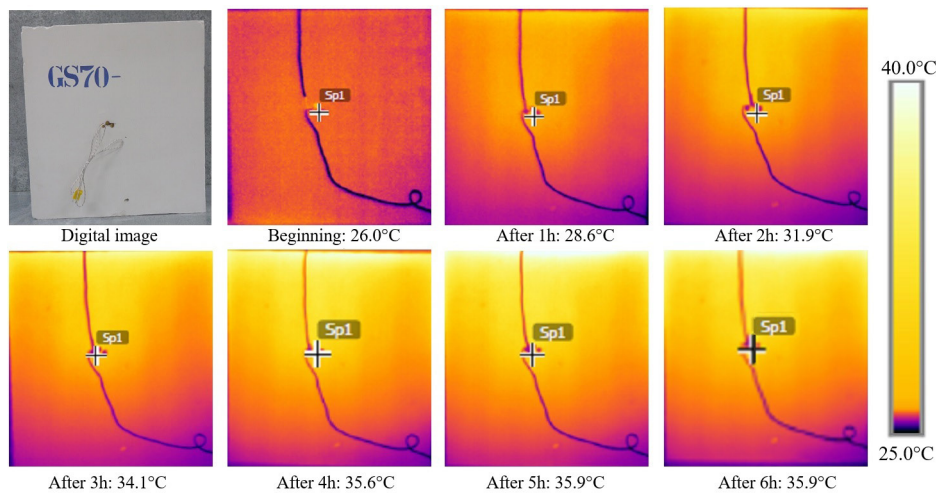


FIGURE 11. GS 70 - heating thermograms.

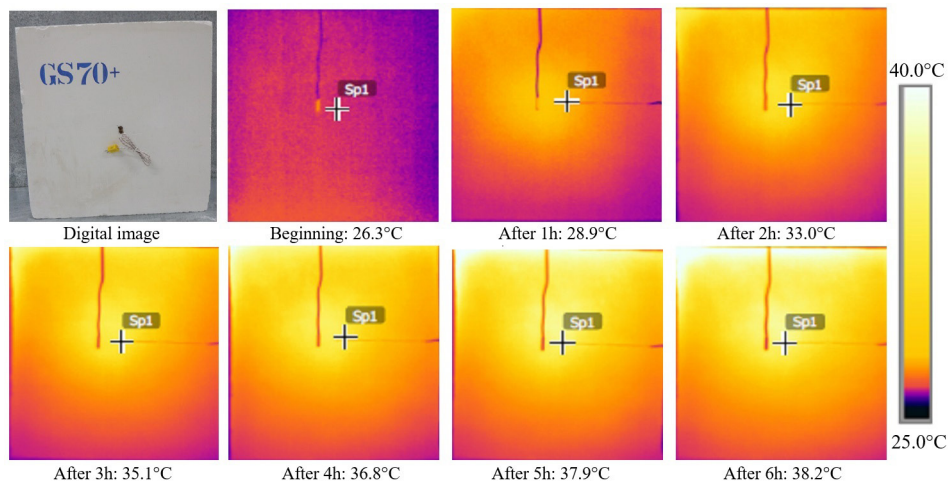


FIGURE 12. GS 70 + heating thermograms.

behavior more than the other hollow elements, as in Figure 10, and in the behavior scheme (Figure 9).

The possibility of visualizing the heat distribution and transmission by the thickness of the element over time was impossible due to the shape and opacity of the walls in the thermal chamber. In view of this, after the removal of the chamber, this visualization will become possible and allow relevant analyzes on the test.

The side view of the plaster block test element GS 100 + is shown in Figure 13 in digital image (upper left corner) and in thermal images during cooling. Four points were selected: 2 at the ends and 2 in the central part. It was possible to observe how the heat transfer occurs in the block by conduction and from it to the environment by convection, predominantly. When the test element was removed from the chamber, it was subjected to room temperature, around 26 °C – colder than any of the exposed faces. Besides, the test element itself had heat transfer still occurring, mostly by conduction. The flow occurs from the point of highest temperature to the lowest; therefore, heat transfer to the environment and between the thermally different points of the test element itself. In Figure 13, point SP1 is closest to the hot (heated) side and SP4 to the cold side.

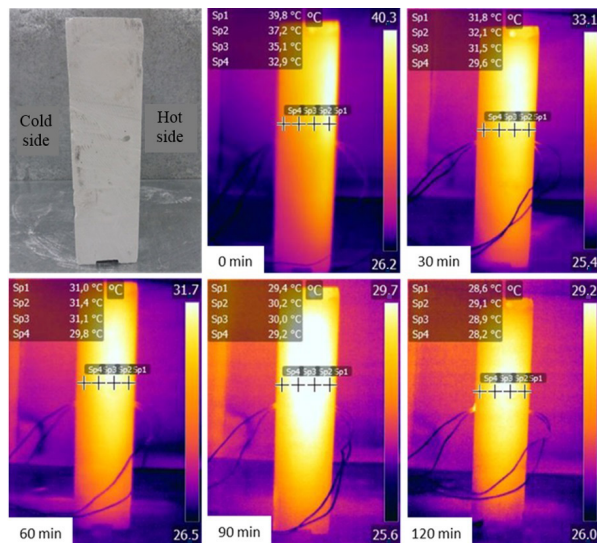


FIGURE 13. Thermograms side view: GS 100 + cooling.

Regarding the thermogram of 0 min, a lighter stain appears, indicating a warmer region. This is because this thermogram is made as soon as the test element has been removed from the thermal chamber, right after the influence of the heat source. In the following thermograms, it is possible to see that this stain “moves” towards the side center of the test element. Then, in the 90 min thermogram, a symmetrical temperature balance occurs, with the most heated points in the center. With the heat convection,

the cooling tends to occur in a similar way in the two main directions. As cooling time happens, the temperatures tend to present a “normal” curve shape, considering, for this test, that room temperatures on both main faces are equal (temperature of the same environment). It is noteworthy that the cooling of the walls usually occurs under different room temperature values. Consequently, the heat flow tends to be different with greater temperature difference; it can become balanced when the external and internal temperatures are equal. Previous studies have also used infrared thermography to study plaster thermal during heating and cooling cycles (77, 78). Just like in these studies, infrared thermography allowing dynamic thermal evaluation, and identification of thermic resistance to heat fluxes were observed.

4. CONCLUSIONS

This work investigated the thermal properties and behavior of plaster block components. An experimental study were carried out: through a thermal chamber, infrared thermography, and normative parameters. The results achieved aimed to advance the studies on the plaster block and contribute to the debate on materials and construction techniques with a focus on the thermal performance of buildings.

The use of the flowmetry method to obtain the thermal conductivity of the plaster allowed observing values for the high and medium density ranges of plaster blocks. The medium density was around 0.356 W/(m·K), very close to the 0.350 W/(m·K) value suggested by NBR 15520 (20). In addition to thermal conductivity, this method allowed the measurement of the thermal resistance for 8 types of solid and hollow plaster blocks. The values were between 0.16 m²·K/W (50 mm solid block) and 0.30 m²·K/W (100 mm hollow block).

The calculation of thermal parameters using NBR 15220 (20) showed the 100 mm hollow block as the one with the lowest thermal transmittance value; however, it was only 2% smaller than the 100 mm solid block, which in turn has higher values of thermal delay and thermal capacity. Also, the latter showed better thermal behavior in the tests, ending the heating with temperature on the opposite side to the heat around 1.5 °C lower than the similar hollow block.

The thermal chamber developed for this work proved to be efficient for carrying out a heating experiment of test elements of vertical seals. The instrumentation used to control, measure, and record temperature through a dimmer, thermocouple, and digital thermometer with the data logger, respectively, allowed verifying and comparing the behavior of the components, without major failure. From the curves generated every minute during 360 minutes of heating, the different thermal behaviors between

the 8 types of plaster blocks were observed. It was possible to conclude that the presence of small voids associated with great thicknesses tends to make these blocks the ones that show superior thermal behavior.

The calculations of the thermal parameters corroborated with the results of the thermal chamber test, with few variations in the order of performance of the blocks. The use of thermography during the tests proved to be relevant and pertinent since it was possible to visualize the temperature distribution superficially: it expands the scope of the point analysis obtained by contact thermocouple and digital thermometer. The thermal behavior of the laying joints in the mini-wall test elements was noticed as well as the voids in the elements with the presence of septa or alveoli. Additionally, through thermography, it was possible to qualitatively analyze the distribution of heating from the heat source and the losses from small cracks in the experimental apparatus.

AUTHOR CONTRIBUTIONS:

Conceptualization: P.I.B. Batista. Data curation: P.I.B. Batista. Formal analysis: P.I.B. Batista, J.H.A. Rocha. Funding acquisition: Y.V. Póvoas. Investigation: P.I.B. Batista, J.H.A. Rocha. Methodology: P.I.B. Batista, J.H.A. Rocha, Y.V. Póvoas. Project administration: Y.V. Póvoas. Resources: Y.V. Póvoas. Validation: P.I.B. Batista, J.H.A. Rocha. Visualization: P.I.B. Batista, J.H.A. Rocha, Y.V. Póvoas. Writing, original draft: P.I.B. Batista, J.H.A. Rocha. Writing, review & editing: P.I.B. Batista, J.H.A. Rocha, Y.V. Póvoas.

REFERENCES

- European Union (2010). Directive 2010/31/EU of the European parliament and of the council of 19 May 2010 on the energy performance of buildings (EPBD recast). Off. J. Eur. Union 2010, 53. Retrieved from <https://eur-lex.europa.eu/LexUriServ/LexUriServ.do?uri=OJ:L:2010:153:0013:0035:EN:PDF>
- Byrne, A.; Byrne, G.; Robinson, A. (2017) Compact facility for testing steady and transient thermal performance of building walls. *Energy Build.* 152, 602-614. <https://doi.org/10.1016/j.enbuild.2017.07.086>.
- Geraldi, M.S.; Ghisi, E. (2020) Building-level and Stock-level in contrast: a literature review of the energy performance of buildings during the operational stage. *Energy Build.* 211, 109810. <https://doi.org/10.1016/j.enbuild.2020.109810>.
- Marinakis, V. (2020) Big data for energy management and energy-efficient buildings. *Energies.* 13 [7], 1555. <https://doi.org/10.3390/en13071555>.
- Al-Naghi, A.A.A.; Rahman, M.K.; Al-Amoudi, O.S.B.; Al-Dulaijan, S.U. (2020) Thermal performance evaluation of walls with aac blocks, insulating plaster, and reflective coating. *J. Energy Eng.* 146, 04019040. [https://doi.org/10.1061/\(asce\)jey.1943-7897.0000636](https://doi.org/10.1061/(asce)jey.1943-7897.0000636).
- Ascione, F.; Bianco, N.; de Masi, R.F.; Mauro, G.M.; Vanoli, G.P. (2015) Design of the Building Envelope: A novel multi-objective approach for the optimization of energy performance and thermal comfort. *Sustainability.* 7 [8], 10809. <https://doi.org/10.3390/su70810809>.
- Lamberts, R.; Duarte, V.C.P. (2016) Desempenho térmico de edificações, Universidade Federal de Santa Catarina, Florianópolis, Brazil.
- Echarri, V.; Espinosa, A.; Rizo, C. (2017) Thermal transmission through existing building enclosures: destructive monitoring in intermediate layers versus non-destructive monitoring with sensors on surfaces. *Sensors.* 17 [12], 2848. <https://doi.org/10.3390/s17122848>.
- Economidou, M.; Todeschi, V.; Bertoldi, P.; Agostino, D.; Zangheri, P.; Castellazzi, L. (2020) Review of 50 years of EU energy efficiency policies for buildings. *Energy Build.* 225, 110322. <https://doi.org/10.1016/j.enbuild.2020.110322>.
- Pereira, B.M.S. (2014) A eficiência energética em edifícios: análise comparativa da regulamentação aplicável na península Ibérica, Master's Thesis, Instituto Politécnico de Viana do Castelo, Viana do Castelo, Brazil.
- Najjar, M.; Figueiredo, K.; Hammad, A.W.A.; Haddad, A. (2019) Integrated optimization with building information modeling and life cycle assessment for generating energy efficient buildings. *Appl. Energy.* 250, 1366–1382. <https://doi.org/10.1016/j.apenergy.2019.05.101>.
- Aguilera, D.G.; Lagüelab, S.; Rodríguez-Gonzálveza, P.; Hernández-López, D. (2013) Image-based thermographic modeling for assessing energy efficiency of buildings façades. *Energy Build.* 65, 29-36. <https://doi.org/10.1016/j.enbuild.2013.05.040>.
- International Organization for Standardization - ISO (2017). ISO 52000-1:2017. Energy performance of buildings — Overarching EPB assessment — Part 1: General framework and procedures. Geneva, Switzerland.
- International Organization for Standardization - ISO (2017). ISO 52003-1:2017. Energy performance of buildings — Indicators, requirements, ratings and certificates — Part 1: General aspects and application to the overall energy performance. Geneva, Switzerland.
- International Organization for Standardization - ISO (2017). ISO 52010-1:2017 Energy performance of buildings — External climatic conditions — Part 1: Conversion of climatic data for energy calculations. Geneva, Switzerland.
- International Organization for Standardization - ISO (2017). ISO 52016-1:2017. Energy performance of buildings — Energy needs for heating and cooling, internal temperatures and sensible and latent heat loads — Part 1: Calculation procedures. Geneva, Switzerland.
- International Organization for Standardization - ISO (2017). ISO 52018-1:2017. Energy performance of buildings — Indicators for partial EPB requirements related to thermal energy balance and fabric features — Part 1: Overview of options. Geneva, Switzerland.
- Tubelo, R.C.S.; Rodrigues, L.T.; Gillot, M.A. (2014) Comparative study of the brazilian energy labelling system and the passivhaus standard for housing. *Buildings.* 4 [2], 207-221. <https://doi.org/10.3390/buildings4020207>.
- Bogo, A.J. (2016) Reflexões críticas quanto as limitações do texto das normas brasileiras de desempenho NBR 15220-3 e NBR 15575. *Holos.* 32, 290-298. <https://doi.org/10.15628/holos.2016.4389>.
- Associação Brasileira de Normas Técnicas (2005) NBR 15220: Desempenho térmico de edificações - Parte 1-5. ABNT, Rio de Janeiro.
- Associação Brasileira de Normas Técnicas (2013) NBR 15575: Edificações habitacionais – Desempenho - Parte 1 -5. ABNT, Rio de Janeiro.
- Instituto Nacional de Metrologia, Normalização e Qualidade Industrial (2012) Regulamento técnico da qualidade para o nível de eficiência energética edificações residenciais (RTQ-R), INMETRO, Rio de Janeiro, Brasil, 2012.
- Marques, T.H.T.; Chavatala, K.M.S. (2013) Review of the Brazilian NBR 15575 standard: applying the simulation and simplified methods for evaluating a social house thermal performance. Proceedings of the Symposium on Simulation for Architecture and Urban Design. San Diego: SimAUD.
- Dalbem, R.; Grala da Cunha, E.; Vicente, R.; Figueiredo, A.; Oliveira, R.; Silva, A.C. (2019) Optimisation of a social housing for south of Brazil: From basic performance standard to passive house concept. *Energy.* 167, 1278–1296. <https://doi.org/10.1016/j.energy.2018.11.053>.
- Silva, E.P.; Melo, A.B.; Queiroga, A.B.R.E. (2013) Desempenho térmico de vedações: estudo comparativo com blocos de eva, tijolo cerâmico e gesso acartonado. Proceedings of the Encontro Nacional de Conforto no Ambiente Construído. Brasília (ENCAC).
- Lakatos, A. (2017) Investigation of the moisture induced degradation of the thermal properties of aerogel blankets:

- Measurements, calculations, simulations. *Energy Build.* 139, 506-516. <https://doi.org/10.1016/j.enbuild.2017.01.054>.
27. Souza, C.R.N. (2015) Estudo da condutividade térmica do gesso (CaSO₄ 0,5 H₂O) em função de sua porosidade. Master's Thesis, Universidade Federal do Vale do São Francisco, Juazeiro, Brazil.
 28. Specht, L.P.; Borges P.A.P.; Rupp, R.F.; Varnier, R. (2010) Análise da transferência de calor em paredes compostas por diferentes materiais. *Amb. Constr.* 10, 7-18. <https://doi.org/10.1590/S1678-86212010000400002>.
 29. Ottelée, M.; Perinib, K. (2017) Comparative experimental approach to investigate the thermal behaviour of vertical greened façades of buildings. *Ecol. Eng.* 108 [Part A], 152-161. <https://doi.org/10.1016/j.ecoleng.2017.08.016>.
 30. Silva, Ê.P.; Cahino, J.E.M.; Melo, A.B. (2012) Avaliação do desempenho térmico de blocos EVA, Proceedings of the Encontro Nacional de Tecnologia no Ambiente Construído, Juiz de Fora (ENTAC).
 31. Allam, R.; Issaadi, N.; Belarbi, R.; El-Meligy, M.; Altahrany, A. (2018) Hygrothermal behavior for a clay brick wall. *J. Heat Mass.* 54, 1579-1591. <https://doi.org/10.1007/s00231-017-2271-5>.
 32. Danieslki, I.; Fröling, M. (2015) Diagnosis of buildings' thermal performance: a quantitative method using thermography under non-steady state heat flow. *Energy Procedia.* 83, 320-329. <https://doi.org/10.1016/j.egypro.2015.12.186>.
 33. Liu, C.; Zhang, Z. (2019) Thermal response of wall implanted with heat pipes: Experimental analysis. *Renew. Energy.* 143, 1687-1697. <https://doi.org/10.1016/j.renene.2019.05.123>.
 34. Bauer, E.; Leal, F.E. (2013) Condicionantes das medições termográficas para avaliação da temperatura em fachadas. Proceedings of the X Simpósio Brasileiro de Tecnologia das Argamassas. Porto Alegre (X SBTA).
 35. Ibañez Puy, M.; Viadurre-Arbizu, M.; Sacristán-Fernández, J.A.; Martín Gómez, F.C. (2017) Opaque Ventilated Façades: Thermal and energy performance review. *Renew. Sust. Energy. Rev.* 79, 180-191. <https://doi.org/10.1016/j.rser.2017.05.059>.
 36. Marques, D.F.P.C. (2014) Avaliação da qualidade térmica da envolvente de edifícios – Estudo de caso através da análise numérica e por termografia infravermelha. Master's Thesis, Faculdade de Ciências e Tecnologias da Universidade Nova de Lisboa, Porto, Portugal.
 37. Kylili, A.; Fokaides, P.A.; Christou, P.; Kalogirou, S.A. (2014) Infrared thermography (IRT) applications for building diagnostics: A review. *Appl. Energy.* 134, 531-549. <https://doi.org/10.1016/j.apenergy.2014.08.005>.
 38. Shariq, M.H.; Hughes, B.R. (2020) Revolutionising building inspection techniques to meet large-scale energy demands: A review of the state-of-the-art. *Renew. Sust. Energy. Rev.* 130, 109979. <https://doi.org/10.1016/j.rser.2020.109979>.
 39. François, A.; Ibos, L.; Feuillet, V.; Meulemans, J. (2021) In situ measurement method for the quantification of the thermal transmittance of a non-homogeneous wall or a thermal bridge using an inverse technique and active infrared thermography. *Energy Build.* 233, 110633. <https://doi.org/10.1016/j.enbuild.2020.110633>.
 40. Lamrani, M.; Laaroussi, N.; Khabbazi, A.; Khalfouli, M.; Garoum, M.; Feiz, A. (2017) Experimental study of thermal properties of a new ecological building material based on peanut shells and plaster. *Case Stud. Constr. Mater.* 7, 294-304. <https://doi.org/10.1016/j.cscm.2017.09.006>.
 41. Rahmanian, I.; Wang, Y.C. (2012) A combined experimental and numerical method for extracting temperature-dependent thermal conductivity of gypsum boards. *Constr. Build. Mater.* 26, 707-722. <https://doi.org/10.1016/j.conbuildmat.2011.06.078>.
 42. Yu, J.; Yang, J.; Xiong, C. (2015) Study of dynamic thermal performance of hollow block ventilated wall. *Renew. Energy.* 84, 145-151. <https://doi.org/10.1016/j.renene.2015.07.020>.
 43. Iucolano, F.; Liguori, B.; Aprea, P.; Caputo, D. (2018) Thermo-mechanical behaviour of hemp fibers-reinforced gypsum plasters. *Constr. Build. Mater.* 185, 256-263. <https://doi.org/10.1016/j.conbuildmat.2018.07.036>.
 44. Uriarte-Flores, J.; Xamán, J.; Chávez, Y.; Hernández-López, I.; Moraga, N.O.; Aguilar, J.O. (2019) Thermal performance of walls with passive cooling techniques using traditional materials available in the Mexican market. *Appl. Therm. Eng.* 149, 1154-1169. <https://doi.org/10.1016/j.applthermaleng.2018.12.045>.
 45. Kheradmand, M.; Azenha, M.; de Aguiar, J.L.; Castro-Gomes, J. (2016) Experimental and numerical studies of hybrid PCM embedded in plastering mortar for enhanced thermal behaviour of buildings. *Energy.* 94, 250-261. <https://doi.org/10.1016/j.energy.2015.10.131>.
 46. Pedreño-Rojas, M.A.; Morales-Conde, M.J.; Pérez-Gálvez, F.; Rodríguez-Liñán, C. (2017) Eco-efficient acoustic and thermal conditioning using false ceiling plates made from plaster and wood waste. *J. Clean. Prod.* 166, 690-705. <https://doi.org/10.1016/j.jclepro.2017.08.077>.
 47. Toppi, T.; Mazzarella, L. (2013) Gypsum based composite materials with micro-encapsulated PCM: Experimental correlations for thermal properties estimation on the basis of the composition. *Energy Build.* 57, 227-236. <https://doi.org/10.1016/j.enbuild.2012.11.009>.
 48. Belayachi, N.; Hoxha, D.; Slaimia, M. (2016) Impact of accelerated climatic aging on the behavior of gypsum plaster-straw material for building thermal insulation. *Constr. Build. Mater.* 125, 912-918. <https://doi.org/10.1016/j.conbuildmat.2016.08.120>.
 49. Bicer, A.; Kar, F. (2017) Thermal and mechanical properties of gypsum plaster mixed with expanded polystyrene and tragacanth. *Therm. Sci. Eng. Prog.* 1, 59-65. <https://doi.org/10.1016/j.tsep.2017.02.008>.
 50. Al-Naghi, A.A.A.; Rahman, M.K.; Al-Amoudi, O.S.B.; Al-Dulajjan, S.U. (2020) Thermal performance evaluation of walls with AAC blocks, insulating plaster, and reflective coating. *J. Energy Eng.* 146, 04019040. [https://doi.org/10.1061/\(asce\)ey.1943-7897.0000636](https://doi.org/10.1061/(asce)ey.1943-7897.0000636).
 51. Batista, P.I.B. (2019). Parâmetros de desempenho térmico de blocos de gesso. Master's Thesis. Escola Politécnica de Pernambuco, Universidade de Pernambuco, Recife, Brazil.
 52. Delgado, J.M.P.Q.; Paula, P. (2018) Hygrothermal performance evaluation of gypsum plaster houses in Brazil. In: J. Delgado, A. Barbosa de Lima (Eds). Transport phenomena in multiphase systems, advanced structured materials. 93, 1-53. United States: Springer. https://doi.org/10.1007/978-3-319-91062-8_1.
 53. Santos, A.N. (2017) Comportamento higrótérmico de paredes em gesso: avaliação da adequabilidade de zonas climáticas do Brasil, PhD Thesis, Faculdade de Engenharia, Universidade do Porto, Porto, Portugal.
 54. Costa e Silva, A.J.; Peres, L. (2016) Como construir: execução de alvenaria não estrutural de blocos de gesso. Revista Techne, Brasil:Pini.
 55. Neves, M.L.R. (2011) Método construtivo de vedação vertical interna com blocos de gesso. Master's Thesis. Escola Politécnica de Pernambuco, Universidade de Pernambuco, Recife, Brazil.
 56. Pires Sobrinho, C.W. (2010) Divisórias internas de edifícios em alvenaria de blocos de gesso- Vantagens técnicas, económicas e ambientais. Proceedings of the Congresso Internacional de Tecnologia Aplicada para a Arquitetura & Engenharia Sustentáveis. Recife.
 57. Associação Brasileira de Normas Técnicas (2017) NBR 16494: Bloco de gesso para vedação vertical — Requisitos. ABNT, Rio de Janeiro.
 58. Associação Brasileira de Normas Técnicas (2017) NBR 13207: Gesso para construção civil - Requisitos. ABNT, Rio de Janeiro.
 59. Associação Brasileira de Normas Técnicas (2019) NBR 12127: Gesso para construção civil — Determinação das propriedades físicas do pó. ABNT, Rio de Janeiro.
 60. Associação Brasileira de Normas Técnicas (2019) NBR 12129: Gesso para construção civil — Determinação das propriedades mecânicas. ABNT, Rio de Janeiro.
 61. American Society for Testing and Materials (2005) ASTM C1363. Standard test method for thermal performance of building materials and envelope assemblies by means of a hot box apparatus. West Conshohocken: ASTM.
 62. Ferrari, S.; Zanotto, V. (2013) The thermal performance of walls under actual service conditions: Evaluating the results of climatic chamber tests. *Constr. Build. Mater.* 43, 309-316. <https://doi.org/10.1016/j.conbuildmat.2013.02.056>.

63. FLIR (2014) User's manual FLIR Exx Series, first ed. Wilsonville: FLIR.
64. Zhao, D.; Qian, X.; Gu, X.; Jajja, S.A.; Yang, R. (2016) Measurement techniques for thermal conductivity and interfacial thermal conductance of bulk and thin film materials. *J. Electron. Packag.* 138 [4], 040802. <http://doi.org/10.1115/1.4034605>.
65. NETZSCH (2010) Operating instructions of Heat Flow Meter HFM 436/6 Lambda, NETZSCH, Selb, Germany.
66. Incropera, F.P.; Dewitt, D.P. (2008) Fundamentos de transferência de calor e de massa, sixth ed., Rio de Janeiro: Guanabara Koogan.
67. Callister, W.; Rethwisch, D. (2018) Materials science and engineering: an introduction. New York: Wiley.
68. Correia, C.; Souza, M. (2009) Mechanical strength and thermal conductivity of low-porosity gypsum plates. *Mater. Res.* 12 [1], 95-99. <https://doi.org/10.1590/S1516-14392009000100012>.
69. Huelsz, G.; Barrios, G.; Rojas, J. (2016) Equivalent-homogeneous-layers-set method for time-dependent heat transfer through hollow-block walls. *Appl. Therm. Eng.* 102, 1019-1023. <https://doi.org/10.1016/j.applthermaleng.2016.03.113>.
70. Mansour, M.B.; Soukaina, C.A.; Benhamou, B.; Jabrallah, S.B. (2013) Thermal characterization of a Tunisian gypsum plaster as construction material. *Energy Procedia.* 42, 680-688. <https://doi.org/10.1016/j.egypro.2013.11.070>.
71. Zhang, Y.; Du, K.; He, J.; Yang, L.; Li, Y.; Li, S. (2014). Impact factors analysis on the thermal performance of hollow block wall. *Energy Build.* 75:330-341. <https://doi.org/10.1016/j.enbuild.2014.02.037>.
72. Bianco, L.; Serra, V.; Fantucci, S.; Dutto, M.; Massolino, M. (2015) Thermal insulating plaster as a solution for refurbishing historic building envelopes: First experimental results. *Energy Build.* 95, 86-91. <https://doi.org/10.1016/j.enbuild.2014.11.016>.
73. Asdrubali, F.; D'Alessandro, F.; Baldinelli, G.; Bianchi, F. (2014) Evaluating in situ thermal transmittance of green buildings masonries—A case study. *Case Stud. Constr. Mater.* 1, 53-59. <https://doi.org/10.1016/j.cscm.2014.04.004>.
74. Simões, I.; Simões, N.; Tadeu, A. (2012) Thermal delay simulation in multilayer systems using analytical solutions. *Energy Build.* 49, 631-639. <https://doi.org/10.1016/j.enbuild.2012.03.005>.
75. Tadeu, A.; Moreira, A.; António, J.; Simões, N.; Simões, I. (2014) Thermal delay provided by floors containing layers that incorporate expanded cork granule waste. *Energy Build.* 68, 611-619. <https://doi.org/10.1016/j.enbuild.2013.10.007>.
76. He, Z.; He, Z.; Zhang, X.; Li, Z. (2015) Study of hot air recirculation and thermal management in data centers by using temperature rise distribution. *Build. Simul.* 9, 541-55. <https://doi.org/10.1007/s12273-016-0282-7>.
77. de Freitas, S.S.; de Freitas, V.P.; Barreira, E. (2014) Detection of façade plaster detachments using infrared thermography—A nondestructive technique. *Constr. Build. Mater.* 70, 80-87. <https://doi.org/10.1016/j.conbuildmat.2014.07.094>.
78. Theodorakeas, P.; Avdelidis, N.P.; Cheilakou, E.; Kouli, M. (2014) Quantitative analysis of plastered mosaics by means of active infrared thermography. *Constr. Build. Mater.* 73, 417-425. <https://doi.org/10.1016/j.conbuildmat.2014.09.089>.